CHAPTER II

BASIC PRINCIPLES OF ERBIUM-DOPED FIBER AMPLIFIERS

2.1 INTRODUCTION

Erbium-doped fiber amplifiers (EDFAs) can be viewed as lasers (EDFLs) operating in the particular regime before occurrence of coherent oscillation of amplified spontaneous emission (ASE) due to some means of feedback. EDFAs are used as travelling-wave amplifiers for coherent light signal regeneration. In this chapter, a description of principles of EDFAs will be presented.

2.2 DOPED GLASS STRUCTURES AND PROPERTIES

In general, when a liquid material is cooled down gradually, it will change to crystal, expelling the specific latent heat at the melting temperature. On the other hand, glass is an inorganic product of fusion cooled to a rigid condition without crystallizing. It is unstable from a thermodynamic standpoint because the enthalpy of the glassy state is higher than that of a crystal state. Therefore, glasses have a short-range order and form a three-dimensional matrix but lack the uniformity, symmetry and structure of a crystalline material and therefore no long-range periodicity.

The glass lattice is built from basic structural units made of network former atoms. The most common is the silica tetrahedron $(SIO_4)^{2-}$. Other usual glass formers

are SiO_2, GeO_2, B_2O_3, P_2O_5, As_2O_3, and Sb_3O_3. Network formers are all capable of forming a three-dimensional network with oxygen, thus providing the very strong covalent bonds that give glasses their characteristic properties.

Fig. 2.1 shows two-dimensional structure analogies for (a) crystal silica and (b) silica glass. The filled circles represent silicon atoms and the open circles represent oxygen atoms. Silicon atoms have one more bond with an oxygen atom and form a three-dimensional structure. The atomic arrangement of silica glass is similar to the crystalline form of silica, but the structure of silica glass, being slightly more random, leads to the lack of long-range periodicity or symmetry.

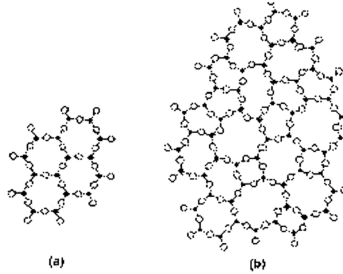

Fig. 2.1 *Two-dimensional structure analogies for*
(a) Crystal silica
(b) Silica glass [1]

The silica-oxygen glass structure is disrupted by the introduction of network modifiers. Oxides of alkali metals and alkali-earth metals such as LIO, Na_2O, K_2O, Rb_2O, Cs_2O, CaO, SrO, and BaO are typical network modifiers. When these elements are added to the glass, the silicon-oxygen structure is opened up (Fig. 2.2) lowering

the density of the glass, weakening the bond strength and lowering the fusion temperature and the viscosity of the glass. The addition of network modifiers is important as it allows glass to be processed at workable temperatures.

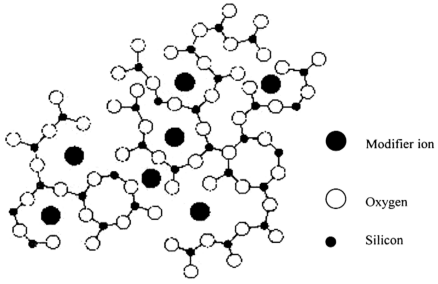

Fig. 2.2 *Schematic diagram of the glass matrix disrupted by the addition of network modifier ions [1].*

Other elements, such as germanium, aluminum, phosphorus, or boron, may substitute a number of silica sites in fused silica. If silica is replaced by germanium, the tetrahedral structure is retained and its properties are similar to fused silica glass. The presence of germanium increases the refractive index over that of the cladding glass and enables a wide range of guiding structures to be made. In fiber for telecommunications, aluminum has been used as an alternative to germanium for increasing the refractive index of the core.

In the oxide glass category, phosphate glasses activated by Nd^{3+} and Er^{3+} have received much attention due to its properties of thermal stability and chemical strength in high power applications. Phosphorus is commonly used in conjunction

with fluorine to dope the silica, giving a cladding material with the same refractive index of the process temperature.

When doped into a glass matrix, rare earth ions are generally in the trivalent state, i.e. the atom has three electrons from other electronic configuration of $4f^n\ 5s^2\ 5p^6$ where n is an integer ranging from 1 for Cerium to 13 for Yb^{3+}. 4f electrons are shielded by the $5s^2$ and $6p^6$ electrons. Therefore, 4f electrons are weakly perturbed by the crystal field (ligand field) of the host. This gives rise to the comparatively sharp energy level structure for transition between the manifold of the 4f electrons.

2.3 ENERGY LEVELS OF Er^{3+} IONS

2.3.1 Stark Effects

When a trivalent rare-earth (RE) ion is excited by an external energy field such as light, the electron charge distribution around the nucleus is altered to that of higher energy states, which are quantized. The states are generally characterized by the Russell-Saunders notation $^{2S+1}L_J$, where 2S+1 is the spin multiplicity of the state, L the total orbital angular momentum and J the total angular momentum quantum number. Dieke and Crosswhite [2] explained the energy level splitting by Coulumbic interaction. Both effects give the typical splitting of the order of a few thousand cm^{-1}. However, Russell-Saunders coupling scheme is valid only when the size of the coulumbic interaction is much greater than the spin-orbit effects.

The $^{2S+1}L_J$ states of the RE ion are further split by the action of the crystal field (ligand field) of the host material into new "Stark levels". Site to site variations of the field due to the amorphous nature of the glass results in an inhomogeneous broadening of the transition [3]. For ions with an even number of electrons the $^{2S+1}L_J$ should split into a multiplet of 2J+1 Stark levels. For an ion with an odd number of

electrons, Kramer's rule [4] limits the number of nondegenerate Stark levels to J+1/2. The actual number of sub-levels observed is, however, dependent on the symmetry of the crystal field and thus the host material. In addition, the magnitude of the energy splitting depends on the magnitude of local electrical fields, which varies depending on their location. Therefore, the Stark splitting in glass materials varies depending on the location of the ions and hence the host field magnitude. Consequently, different condensed materials such as silica glass, fluoride glass, and crystal provide individual, different spectral characteristics of absorption and fluorescence of RE ions because of their different Stark split energy levels.

Fig. 2.3 shows the diagram of energy levels and Stark splitting of Er^{3+} ion. Intra-manifold thermalization enables a constant population distribution to be maintained within the manifolds (Boltzmann's distribution) [5]. The eightfold and sevenfold Stark splitting of the ground ($^4I_{15/2}$) and upper ($^4I_{13/2}$) levels, respectively, combined with the effect of inhomogeneous broadening makes Er^{3+}: glass a rather complicated multilevel laser-system.

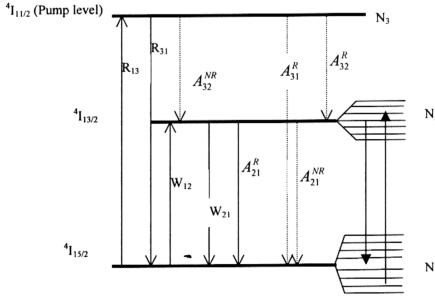

Fig. 2.3 *Energy levels of Er^{3+} ion*

2.3.2 Rate Equations

Er^{3+}-doped fiber is a three-level laser system when pumped to the $^4I_{11/2}$ level with 980 nm light as shown in Fig. 2.3. $^4I_{15/2}$ state is defined as the ground level, $^4I_{13/2}$ is the metastable level characterized by a long lifetime τ, which depends on the concentration of erbium ions as well as ambient temperature [6-7]. The laser transition takes place between $^4I_{13/2}$ -$^4I_{15/2}$ states.

The pumping rate from $^4I_{15/2}$ and $^4I_{11/2}$ is denoted as R_{13} and stimulated emission rate between $^4I_{11/2}$ and $^4I_{15/2}$ is R_{31}. There are two possibilities of decay from the excited state ($^4I_{11/2}$), i.e., radiative (rate $A_3^R = A_{32}^R + A_{31}^R$) and nonradiative (rate A_{32}^{NR}). The spontaneous decay from $^4I_{11/2}$ is assumed to be predominantly nonradiative, i.e., $A_{32}^{NR} >> A_3^R$ since the separation between the two upper levels is small (~ 3.4 cm^{-1}) and the lifetime is extremely fast (~ 10^{-6} s). W_{12} and W_{21} represent the stimulated absorption and emission rates respectively between $^4I_{15/2}$ and $^4I_{13/2}$ states. The spontaneous decay from the metastable level is $A_{21} = A_{21}^R + A_{21}^{NR}$ with $A_{21}^R = 1/\tau$, where τ is the fluorescence lifetime. It is assumed that the spontaneous decay is essentially radiative, i.e., $A_{21}^R >> A_{21}^{NR}$.

Therefore, the atomic rate equations are given by [5]:

$$\frac{dN_1}{dt} = -R_{13}N_1 + R_{31}N_3 - W_{12}N_1 + W_{21}N_2 + A_{21}N_2 \tag{2.1}$$

$$\frac{dN_2}{dt} = W_{12}N_1 - W_{21}N_2 - A_{21}N_2 + A_{32}N_3 \tag{2.2}$$

$$\frac{dN_3}{dt} = R_{13}N_1 - R_{31}N_3 - A_{32}N_3 \tag{2.3}$$

$$\rho_0 = N_1 + N_2 + N_3 \tag{2.4}$$

where ρ_0 is the laser ion density and N_1, N_2 and N_3 the populations of atoms in the energy states $^4I_{15/2}$, $^4I_{13/2}$ and $^4I_{11/2}$ respectively.

At steady state, $\frac{dN_1}{dt} = \frac{dN_2}{dt} = \frac{dN_3}{dt} = 0$. By assuming that the nonradiative decay rate A_{32} dominates are the pumping rate $R_{13,31}$, i.e., $A_{32} >> R_{13,31}$, then the solution of Eq. (2.1) and (2.2) are

$$N_1 = \rho_0 \frac{1 + W_{21}\tau}{1 + R\tau + W_{12}\tau + W_{21}\tau} \tag{2.5}$$

$$N_2 = \rho_0 \frac{R\tau + W_{12}\tau}{1 + R\tau + W_{12}\tau + W_{21}\tau} \tag{2.6}$$

$$N_3 \approx 0 \tag{2.7}$$

where $R = R_{13}$. The pump level population is negligible due to the extremely fast nonradiative decay (A_{32}) toward the metastable level $^4I_{13/2}$.

The population inversion per unit volume is defined as

$$\Delta N = N_2 - N_1 = \frac{R\tau + W_{12}\tau - 1}{1 + R\tau + W_{12}\tau} \rho \tag{2.8}$$

with $W_{21} \approx 0$ before the threshold is reached. Therefore, the relative population inversion is:

$$n_{th} = \frac{\Delta N}{\rho} = \frac{R\tau + W_{12}\tau - 1}{1 + R\tau + W_{12}\tau} \geq 0 \tag{2.9}$$

Pumping rate R becomes:

$$R = \frac{W_{12}(1 - n_{th})\tau - (1 + n_{th})}{(n_{th} - 1)\tau} \tag{2.10}$$

Since a small excess population inversion over unity is needed in order to sustain oscillation, therefore, in this condition,

$$R_{th} \approx \frac{1 - W_{12}\tau}{\tau} \tag{2.11}$$

It means that long fluorescence lifetimes ensure a low threshold of oscillation.

2.3.3 Nonradiative Relaxation

Radiative relaxation processes of an excited ion via the emission of photons had been discussed in the previous section. This section will be limited to nonradiative relaxation chiefly due to multiphonon decay. The interpretation is that the energy is being emitted nonradiatively to the lattice as phonon. An excited state *i* has a lifetime of [8]

$$\frac{1}{\tau_i} = \sum_j W_{ij}^R + \sum_j W_{ij}^{NR} \tag{2.12}$$

where W_{ij}^R denotes the probability of radiative decay from level *i* to j and W_{ij}^{NR} the corresponding probability for nonradiative decay. At low temperature, the empirical "energy gap law" states that the multiphonon nonradiative decay rate is given by [8-9]:

$$W_{NR} = We^{-\alpha \Delta E} \tag{2.13}$$

where W and α are positive constants dependent upon the host material and the strength of the ion-lattice coupling, and ΔE is the energy difference between the initial and final state. This energy is different in different crystal hosts [9].

Nonradiative multiphonon decay rates also vary with temperature [9]. With increasing temperature, induced phonon emission becomes important [6]. In order to determine multiphonon emission rates, Riseberg and Moos [9] developed a phenomenological model based on perturbation theory. This model assumes that only phonons of a single frequency are used for the nonradiative transition. Nonradiative multiphonon emission rate $W_{NR}(T)$ in this model is given by

$$W_{NR}(T) = W_0(n_i + 1)^{P_i} \tag{2.14}$$

where W_0 is the low temperature spontaneous multiphonon emission rate that is determined by substituting the radiative probability from the temperature-independent lifetime measured at low temperatures [6], P_i is the number of phonon emitted in the transition. n_i is the occupation number of the ith phonon mode which can be replaced by the Bose-Einstein average

$$\bar{n}_i = \frac{1}{e^{\frac{h\nu_i}{kT}} - 1} \tag{2.15}$$

where $h\nu_i$ is the energy of the phonon in the ith mode.

As the temperature is raised, phonon modes become thermally populated and the multiphonon transition rate grows because of the stimulated emission of phonons. The temperature-dependent multiphonon transition rate then becomes:

$$W_{NR}(T) = W_0\left(\frac{e^{\frac{h\nu_i}{kT}}}{e^{\frac{h\nu_i}{kT}} - 1}\right)^{P_i} \tag{2.16}$$

The total rate of multiphonon emission arises from contributions of many different combinations of phonon modes and frequencies through the Brillouin zone. Therefore, unless a single narrow-frequency band of high-density phonons dominates the relaxation over an extended temperature range, a simple expression such as Eq. (2.16) is not expected to be totally adequate and some composite temperature-dependence curve should be more appropriate [6].

In addition to decay between multiplets, phonons are also responsible for the depopulation of the highest energy Stark levels within a multiplet (sublevels or manifolds). Emission of low acoustic phonons causes depopulation in the upper manifolds and population to accumulate in the lowest energy Stark levels. Therefore,

the population is distributed among the sublevels according to Boltzmann distribution. This process typically occurs on a time scale of 10^{-10} s and this means that all the emission from a multiplet can be considered to occur mainly from the lowest energy Stark level although the thermal distribution of population throughout the multiplet means that there is a finite probability of a transition occurring from a higher Stark level.

2.3.4 Pump Bands and Excited/Ground State Absorption

There are many pump bands for Er-doped fibers such as the 660 nm, 820 nm 980 nm and 1480 nm that have potential for highly efficient pumping [10-11]. The 980 nm and 1480 nm bands are being investigated intensively because high gain characteristics have been easily obtained with those wavelengths. Fig. 2.4(a) shows the energy levels corresponding to each possible atomic sate $^{2S+1}L_J$ for Er : glass. The figure also shows possible absorption transitions in the visible and infrared pump bands and possible radiative transitions. The corresponding absorption spectrum is illustrated in Fig. 2.4(b). The broad and intense absorption band near 1530 nm indicates that Er : glass is a strongly absorbing medium when not activated by any pumping mechanism.

The disadvantage of the short wavelength pump bands is that efficient pumping is severely impeded by pump excited state absorption (ESA). Fig. 2.4(c) shows the energy level diagram of ground state and excited state transitions. In the effect of pump ESA, the pump light at frequency ν_p is not absorbed from the ground level (1) of the rare earth ion, but from an excited level (2), due to the existence of a third level (3) whose energy gap $\Delta E = E_3 - E_2$ with level 2 happens to closely match the pump photon energy $h\nu_p$. This process happens only if the ESA cross section

overlaps with the ground state absorption (GSA) or pump cross section. For example, for the pump band of 820 nm, ESA is caused by $^4I_{13/2} - {}^4S_{3/2}$ transition which has an absorption peak at 850 nm. At a shorter pump band of 660 nm, ESA originated from $^4I_{13/2} - {}^4F_{3/2}$ and $^4I_{13/2} - {}^4F_{5/2}$ transition can be observed at 630 nm [10].

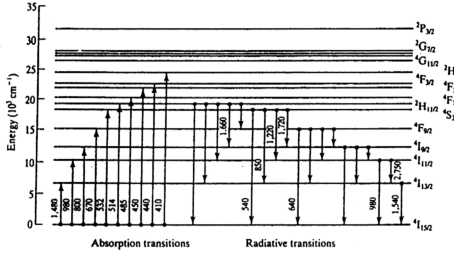

(a)

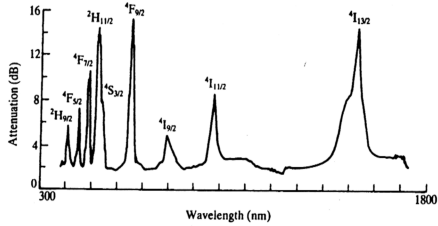

(b)

(continue...)

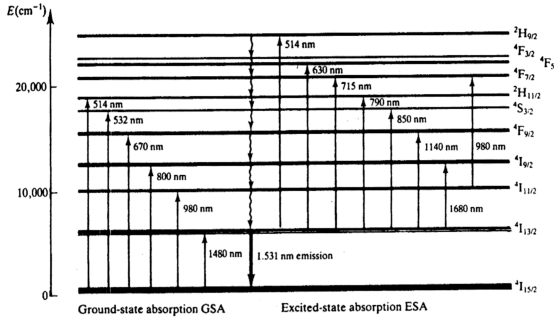

(c)

Fig. 2.4 *Spectroscopy of Er^{3+} in glass. (a). Energy level diagram of Er : glass showing absorption and radiative transmission. (b). Typical absorption spectrum of aluminosilicate Er-doped fiber. (c) Energy level diagram showing GSA and ESA transitions [5].*

2.4 BROADENING

There are two types of mechanism responsible for the broadening of the optical transition in the RE doped glasses: *homogeneous* and *inhomogeneous* broadening. It is assumed that the homogeneous broadening of the laser transitions between the two J manifolds far exceeds the inhomogeneous broadening due to the random glass structure. This is the case at room temperature for most RE ions in glass, because of the broadening effect of phonon coupling [12].

Homogeneous Broadening

Homogeneous broadening of a transition can originate both from the finite lifetime of the initial and final states of a transition and from the dephasing time resulting from fluctuations in the optical transition frequency. The former reason can

be explained by the uncertainty principle, $\Delta E \Delta \tau \approx h$, where ΔE and $\Delta \tau$ are uncertainties of energy and lifetime respectively. The fluctuation in the optical transition frequency results from interactions of ions with phonons. These interactions do not terminate the lifetime of the ion in its absorbing or emitting state but interrupt the relative phase of the ionic oscillation and that of the corresponding field and this causes a broadening of the response time again according to the uncertainty principle where τ represents the mean time between interactions. The room temperature homogeneous linewidth of a transition in glass is of the order of a few tens cm^{-1} and has a strong variation with glass composition and temperature [1,5].

Inhomogeneous Broadening

Since the frequency of a particular transition on the ion is influenced by ligand fields, a range of transition frequencies may be expected and the line is said to be inhomogeneously broadened. Inhomogeneous broadening results from the site-to-site variation in the ligand field as a result of strain, defects, dislocation and lattice impurity in the glasses as well as the presence of other impurities known as network modifiers in addition to the RE dopant. This causes a randomization of the Stark effect, changing the energy positions of the Stark sublevels. The surrounding electric filed also affects the electric dipole transition characteristics. The resultant effect is that different laser line characteristics are exhibited. The typical inhomogeneous linewidth of a transition in a RE doped glass is of the order of 8-49 cm^{-1} [5].

2.5 SPONTAEOUS AND STIMULATED EMISSION

Optical transitions between two energy level having energies E_2 and E_1 and population N_2 and N_1 may occur spontaneously or by stimulation of electromagnetic

radiation in the appropriate frequency region. The increase of power by stimulated emission is a coherent process since it simply increases the existing excitation of the radiation mode at a range that is proportional to the energy already stored in that mode. Spontaneous emission, on the other hand, is inherent in having no relation with the already existing excitation, and occurs at a rate independent of the energy stored in that mode.

The absorption rate from the ground state may be written as

$$\beta_{12} N_1 \delta(\nu_{12}) \tag{2.17}$$

where $\delta(\nu_{12})$ is the energy density of the corresponding frequency $\nu_{12} = (E_2 - E_1)/h$ and β_{12} is the Einstein's coefficient of stimulated absorption. From the excited state the Er^{3+} ions may return to the ground state by spontaneous emission with a rate of

$$A_{21} N_2 \tag{2.18}$$

or by stimulated emission with a rate of

$$\beta_{21} N_2 \delta(\nu_{12}) \tag{2.19}$$

where A_{21} and β_{21} are the Einstein's coefficient of spontaneous and stimulated emission, respectively. Under thermal equilibrium conditions,

$$\beta_{12} N_1 \delta(\nu_{12}) = A_{12} N_2 + \beta_{21} N_2 \delta(\nu_{12}) \tag{2.20}$$

Using the Boltzmann relation

$$\frac{N_2}{N_1} = \exp(\frac{-h\nu_{12}}{kT}) \tag{2.21}$$

The radiation density $\delta(\nu_{12})$ becomes

$$\delta(\nu_{12}) = \frac{A_{21}}{B_{12} \exp(\frac{h\nu_{12}}{kT}) - B_{21}} \tag{2.22}$$

By comparing the Eq. (2.31) with Planck's Law

$$\delta(\nu) = \frac{8\pi h\nu^3}{c^3} B_{12} \tag{2.23}$$

we obtain

$$B_{21} = B_{12} \tag{2.24}$$

and

$$A_{21} = \frac{8\pi h\nu^3}{c^3} B_{12} \tag{2.25}$$

This equation is valid in vacuum for particles having non-degenerate energy levels. When the energy levels are degenerate the Einstein relation (2.24) takes the form

$$g_1 B_{12} = g_2 B_{21} \tag{2.26}$$

where g_1 and g_2 are the degeneracies of level 1 and 2, respectively. In glass, the index of refraction $n \neq 1$, therefore Eq. (2.25) becomes:

$$A_{21} = \frac{8\pi h\nu^3 n^3}{c^3} B_{12} \tag{2.27}$$

In the case of EDFA, the Er^{3+} ion is excited from the ground state through absorption of pump light and decays nonradiatively from the upper level of $^4I_{11/2}$ (in the case of 980 nm pump) until it reaches the metastable state ($^4I_{13/2}$). The incident signal light arrives at the excited erbium atoms distributed along the optical fiber core. Stimulated emission occurs creating additional photons with the same optical phase and direction as the incident signal, thus amplification is realized. Excited ions that do not interact with the incident light spontaneously decay to the ground state with a time constant of approximately 10 ms, depending on the host materials used. The captured spontaneous emission (SE) has a random phase and direction. Typically less than 1% of the SE is captured by the optical fiber mode and becomes a source of optical noise. This noise gets amplified resulting in *amplified spontaneous emission (ASE)*.

The generated ASE power propagates in both fiber directions (ie., forward and backward, with respective to the signal propagation direction). In the unsaturated gain regime (small-signal gain regime), the output ASE in a given bandwidth $\Delta\nu$ of an amplifier with gain G can be expressed as:

$$P_{ASE}^{\pm} = n_{sp}^{\pm} h\nu_s (G-1) = n_{eq}^{\pm} h\nu_s \Delta\nu G \tag{2.28}$$

where $n_{sp}^{\pm}$ and $n_{eq}^{\pm}$ are, the *spontaneous emission factor* and the *equivalent input noise*, respectively, corresponding to forward and backward propagation directions. Spontaneous emission factor becomes irrelevant when the amplifier gain is less than or equal to unity. In the high gain regime and complete inversion limit ($N_1 \approx 0$) with strong pumping in the 980 nm band, the spontaneous emission factor reaches its minimum value:

$$n_{sp}^{\pm} \approx n_{eq}^{\pm} \approx 1 \tag{2.29}$$

since

$$n_{sp} = \frac{\sigma_e N_2}{\sigma_e N_2 - \sigma_a N_1} \tag{2.30}$$

where $\sigma_{a,e}$ = absorption (emission) cross section.

2.6 ABSORPTION AND SMALL-SIGNAL GAIN COEFFICIENT

In the absorption of light the decrease of light intensity passing through material of thickness dx is given by

$$I(\nu, x) = I_0 e^{-\gamma(\nu)x} \tag{2.31}$$

where $\gamma(\nu)$ is the absorption coefficient.

The relation between the integrated absorption coefficient γ and spontaneous emission coefficient A_{21} is given by the Fuchtbauer-Ladenburg formula [13]:

$$\int \gamma(\nu) d\nu = \frac{\lambda^2}{8\pi n^2 \tau} \frac{g_2}{g_1} (N_1 - \frac{g_1}{g_2} N_2) \tag{2.32}$$

Here, the radiative probability A_{21} is represented by $1/\tau$ where τ is the spontaneous emission lifetime of the emitting level. λ is the peak wavelength of the transition.

When the density of radiation is not very high, all absorption takes place from the ground state denoting the absorption of the totally unexcited material by $\gamma(\nu)$, then

$$\int \gamma(\nu) d\nu = \frac{\lambda^2}{8\pi n^2 \tau} \frac{g_2}{g_1} \rho_0 \tag{2.33}$$

where ρ_0 is the total number of Er^{3+} ions per unit volume.

When population inversion takes places between levels 1 and 2, the cavity modes experience amplification. The amplification rate, or small-signal gain coefficient, β is expressed as:

$$\beta(\nu) = -\gamma(\nu) \tag{2.34}$$

$$\beta(\nu) = \frac{\lambda^2}{8\pi n^2 \tau} \frac{g_2}{g_1} g(\nu, \nu_0)(\frac{g_1}{g_2} N_2 - N_1) \tag{2.35}$$

where ν_0 is the central frequency.

Hence, the integrated gain coefficient is:

$$\int \beta(\nu) d\nu = \frac{\lambda^2}{8\pi n^2 \tau} \frac{g_2}{g_1} (\frac{g_1}{g_2} N_2 - N_1) \tag{2.36}$$

with the normalisation of

$$\int g(\nu, \nu_0) d\nu = 1 \tag{2.37}$$

2.7 PRINCIPLES OF GAIN-CLAMPING IN ERBIUM-DOPED FIBER AMPLIFIERS

Gain-clamped effect in erbium-doped fiber amplifier (EDFA) systems has been realized by looping back certain portion of the ASE into the system [14-16] to establish a laser oscillation. Therefore, a gain-clamped EDFA is in fact a fiber laser system operating above threshold of self-oscillation. Analysis of the laser behavior at the threshold region is thus necessary to understand the mechanism of the gain-clamping effect in the EDFA system with optical feedback.

Consider a lowest cavity mode with photon number $n(t)$ and an ideal two-level laser transition with metastable-level population $N_2(t)$ pumped at a steady pumping rate of R_p ions/s and to have a population decay rate γ_2.

The coupled rate equations for this system are given by [17]:

$$\frac{dn}{dt} = K(n+1)N_2 - \gamma_c n \tag{2.38}$$

$$\frac{dN_2}{dt} = R_P - KnN_2 - \gamma_2 N_2 \tag{2.39}$$

where γ_c is the cavity decay rate and the coupling constant K is given by $K = 3*\gamma_{rad}/P$ with γ_{rad} denotes the radiative decay rate on the laser transition. The quantity P is the very large number of resonant cavity modes within the transition linewidth. Note that K is simplified to be γ_{rad}/P from here on.

Steady-state Solutions Below Threshold

The steady-state solution to Eq. (2.38) and (2.39) is given in the form

$$n = \frac{N_2}{\frac{\gamma_C}{K} - N_2} = \frac{N_2}{N_{th} - N_2} \tag{2.40}$$

and

$$N_2 = \frac{R_P}{\gamma_2 + N_2} = R_P \tau_2 \times \frac{1}{1 + (\frac{\gamma_{rad}}{\gamma_2})(\frac{n}{P})} \tag{2.41}$$

where $N_{th} = \frac{\gamma_2}{K} = \frac{\gamma_C}{\gamma_{rad}} P$, is the threshold inversion value

$\tau_2 = \frac{1}{\gamma_2}$, is the photon lifetime at the metastable level.

Eqs. (2.40) and (2.41) states that n is small since $N_2 << N_{th}$ for small R_p and $N_2 \propto R_p \tau_2$ since $n << P$.

At the threshold where $N_2 \rightarrow N_{th}$, the pumping rate is thus given by

$$R_{P,th} = \frac{N_{th}}{\tau_2} = \frac{\gamma_2 \gamma_C}{\lambda_{rad}} P \tag{2.42}$$

Define the normalized pumping rate to be

$$r = \frac{R_P}{R_{P,th}} = \frac{\gamma_{rad} R_P}{\gamma_2 \gamma_C P} \tag{2.43}$$

and substitute $N_2 \approx R_p \tau_2$ and $N_{th} = \gamma_c P / \gamma_{rad}$ into Eq. (2.40) giving

$$n = \frac{r}{r-1} \qquad (r < 1, \text{ below threshold}) \tag{2.44}$$

Substituting R_p from Eq. (2.43) into $N_2 \approx R_p \tau_2$ produces

$$N_2 \approx r \times N_{th} \qquad (r < 1, \text{ below threshold}) \tag{2.45}$$

The plots for Eqs. (2.44) and (2.45) are illustrated in Fig. 2.5.

Steady-state Behavior Above Threshold

Rearrange the steady-state solutions to be

$$N_2 = \frac{n}{n+1} \times N_{th} \tag{2.46}$$

$$n = \frac{\gamma_{rad} P}{\gamma_2} [\frac{N_{th}}{N_2} r - 1] \tag{2.47}$$

From Eq. (2.46), it can be seen that above threshold ($r > 1$) where $n >> 1$, the population inversion N_2 "clamps" at the threshold value, that is,

$$N_2 \approx N_{th} \qquad (r > 1, \text{ above threshold}) \tag{2.48}$$

and Eq. (2.47) becomes

$$n \approx (r-1)\gamma_{rad} P / \gamma_2 \quad (r > 1, \text{ above threshold}) \tag{2.49}$$

Figs. 2.6 (a) and (b) show the plot for the population and photon number for the case of above threshold, respectively.

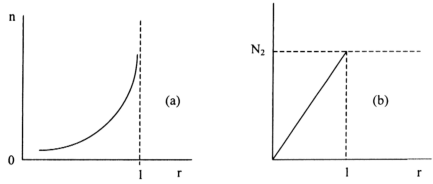

Fig. 2.5 *Below oscillation threshold (a). Photon numbers and (b). Population inversion.*

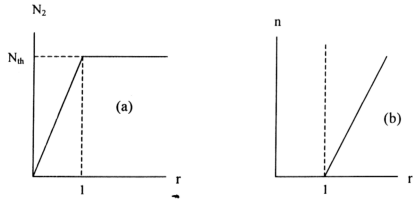

Fig. 2.6 *Laser behavior above threshold. (a) Threshold inversion. (b). Photon numbers.*

Mechanism of Energy Transfer

Below oscillation threshold, all of the pumping power used in exciting erbium ions into the metastable level is reemitted as incoherent energy in the form of radiative relaxation processes (spontaneous emission) and non-radiative relaxation processes (lattice phonon).

Once the onset of laser oscillation takes place, the metastable-level population, N_2 clamps at the threshold value N_{th} and hence the incoherent relaxation out of this level also clamps just at the value it had at threshold. Consequently, a weak probe signal experiences a pumping-rate independent gain since all of the additional pumping power fed into the metastable level above threshold goes into the coherently oscillating cavity mode.

2.8 KEY ISSUES FOR OPTICAL AMPLIFIERS

2.8.1 Signal Gain

Signal gain is the most fundamental parameter of an erbium-doped optical amplifier and an optical amplifier gain, G, is defined as

$$G = \frac{(P_{sout} - P_{ASE})}{P_{\sin}} \tag{2.50}$$

where P_{sin} and P_{sout} are the amplifier input and output signal powers respectively and P_{ASE} is the amplified spontaneous emission (ASE) power. The net amplifier gain, G, can be derived from an analysis of the gain from individual segments along the erbium-doped fiber of length L. An ASE-free two-level approximation is used. The net gain, G, is composed of the contribution of all the gain, $g(z)$ along the fiber, with incremental length Δz [18]:

$$G = \lim_{\Delta z \to 0} \left\{ e^{g(z_1)\Delta z} \times e^{g(z_2)\Delta z} \times \ldots\ldots e^{g(z_n = L)\Delta z} \right\} = \exp\left(\int_0^L g(z)dz \right) \tag{2.51}$$

The gain coefficient is dependent on the metastable level population density, N_2, the ground state population, N_1, the stimulated emission and absorption cross-section, σ_e and σ_a, and the overlap factor or confinement factor, Γ_s:

$$g(z) = \Gamma_s [\sigma_e N_2(z) - \sigma_a N_1(z)] \tag{2.52}$$

Therefore, the net signal gain is

$$G = \exp\{\Gamma_s [\sigma_e N_2 - \sigma_a N_1] L\} \tag{2.53}$$

For complete or near-complete inversion, $N_1 \approx 0$. The maximum signal gain is then

$$G_{\max} \approx \exp(\Gamma_s \sigma_e N_2 L) \tag{2.54}$$

The signal gain can also be derived from concentration of energy [5]. If $\phi_p = P_p/h\nu_p$ is the flux of input pump photons, $\phi_{sin,sout} = P_{sin,sout}/h\nu_s$ the flux of input and output signal photons respectively then

$$\phi_{sout} \le \phi_p + \phi_{\sin}$$

or

$$P_{sout} \le P_{\sin} + \frac{\lambda_p}{\lambda_s} P_p \tag{2.55}$$

by substituting the pump (signal) frequency $\nu_{p,s} = c/\lambda_{p,s}$, where $\lambda_{p,s}$ is the pump (signal) wavelength. For an amplifier free from spontaneous emission, $G = P_{sout}/P_{sin}$, Eq. (2.55) becomes

$$G \le 1 + \frac{\lambda_p}{\lambda_s} \frac{P_p}{P_{\sin}} \tag{2.56}$$

Therefore, the maximum possible amplifier gain is given by the lowest between the two limits obtained in Eq. (2.54) and (2.56)

$$G \le \min\left\{\exp(\rho\sigma_e L), 1+\frac{\lambda_p}{\lambda_s}\frac{P_p}{P_{\sin}}\right\} \tag{2.57}$$

and the maximum possible amplifier output signal power can also be expressed similarly,

$$P_{sout} \le \min\left\{P_{\sin}\exp(\rho\sigma_e L), P_{\sin}+\frac{\lambda_p}{\lambda_s}P_p\right\} \tag{2.58}$$

2.8.2 Noise

Noise figure represents a measure of the signal-to-noise ratio (SNR) degradation for the input to the output of the amplifier. System application requires that a certain level of SNR be achieved at the receiver end. The main contributor to the optical noise of an optical amplifier is from ASE. The total ASE power P_{ASE} is summed over all the spatial modes that the optical fiber supports in an optical bandwidth, B_0 [18]:

$$P_{ASE} = 2n_{sp}h\nu[G(z)-1]B_0 \tag{2.59}$$

where $h\nu$ is the photon energy. The factor of 2 represents two propagating modes of polarization in the LP_{01} mode. The spontaneous emission factor, n_{sp}, as expressed in Eq. (2.30) is given by

$$n_{sp} = \frac{\sigma_e N_2}{\sigma_e N_2 - \sigma_a N_1} \tag{2.60}$$

The ASE power can also be expressed in spectral density (W/Hz) ρ_{ASE}:

$$\rho_{ASE} = 2n_{sp}h\nu[G(z)-1] \tag{2.61}$$

The amplifier optical noise figure NF is defined as [5]:

$$NF = SNR(0)/SNR(z) \tag{2.62}$$

where *SNR(0)* and *SNR(z)* are the signal-to-noise ratio of amplifier at input and fiber co-ordinate z, respectively. The signal-spontaneous beat-limited noise figure is given by

$$NF(z) = \frac{1}{G(z)} + 2n_{sp}\frac{[G(z)-1]}{G} \tag{2.63}$$

or

$$NF(z) = \frac{1}{G(z)} + \frac{\rho_{ASE}}{G(z)h\nu} \tag{2.64}$$

which ignores signal shot noise, ASE beat noise and ASE shot noise. In the high gain limit $G >> 1$, Eq. (2.64) reduces to

$$NF(z, G >> 1) \approx 2n_{sp} \tag{2.65}$$

For strong pumping in the 980 nm band, complete inversion can be achieved, $N_1 \approx 0$. Therefore, from Eq. (2.60), $n_{sp} \approx 1$. This gives the quantum limited of $NF = 2$ (in linear scale) or 3 dB (in log scale). Note that the noise figure performance is mainly determined by the inversion level at the input end of erbium-doped fiber [5, 19].

2.9 SIMULATION USING *OptiAmplifier*

2.9.1 Introduction to *OptiAmplifier* [20]

The modeling work in this study was done using commercial software: *OptiAmplifier* developed by Optiwave. The software finds the population inversion distribution of erbium-doped fiber and the optical spectrum, in both directions, at all points in the system. Different model assumptions can be selected to account for amplifier self-saturation, concentration quenching and Rayleigh scattering.

There are several physical models to calculate the output spectrum from doped fiber in OptiAmplifier:

1. Giles Model [Appendix A]

The Giles model is based on absorption and gain parameters that are proportional to the cross sections. The rate and propagation equations are solved by integrating the spectral evolution back and forth along the fiber until it converges.

2. Saleh's Model

This model estimates output powers by neglecting ASE saturation; it solves for the pump and signal output powers by solving a transcendental equation. The solution is based on absorption and saturation parameters that can be determined from an absorption measurement. Because it does not give the ASE noise spectrum, it breaks down when ASE saturation occurs. But it is useful for providing an initial estimate for use in the Giles model. Saleh's model only provides output powers; it does not provide information about the powers along the doped fiber.

3. Jopson Model

This model solves the Saleh model along the fiber to provide estimates for the powers along the doped fiber and the initial population inversion along the fiber.

4. Equivalent ASE

This model can be used to estimate the equivalent ASE input power. This provides a more accurate initial estimate for use in the Saleh/Jopson model by estimating ASE saturation.

5. Average Inversion Model

The average inversion model for homogeneous saturation provides an estimate for the gain and noise from a doped fiber based on an estimate of the average inversion along the fiber. Using this model, from a reference spectrum and cross section ratio, the gain at any other inversion can be predicted. Although it does not predict how a given population inversion is obtained, i.e. predict the pump power, it is

useful for designing flat-gain amplifiers and for designing systems where the EDFA can be treated as a black box.

OptiAmplifier allows the user to select LP01 or Gaussian mode approximations for the confinement factors, and the power-dependence of the confinement factors. The 3-dimensional calculation can be accelerated, with very little sacrifice to accuracy in most cases, by reducing the number of transverse integrations. These models can be improved at high concentrations by including terms that count for concentration quenching or cross relaxation. Cross relaxation, or ion-ion interactions, increase as the doping concentration increases. In this process, two neighboring excited ions exchange energy so that one ion relaxes back to the ground state. This reduces the quantum efficiency of short, high-concentration amplifiers and lasers. Two models have been proposed for calculating the reduction in population inversion: *OptiAmplifier* allows the user to select the homogeneous or inhomogeneous model or the combination of both.

Temperature dependence was included in the Er-model, enabling the user to predict the gain and other calculated values that characterize the amplifier performance changing under temperature variation. A model, where McCumber's relation has been rewritten in terms of temperature dependence, was implemented and the temperature dependence is embodied in the absorption and emission coefficients or in the cross-sections.

There are three different algorithms that the calculation progresses through to reach the final solution. At each iteration stage, the different spectral can be used for different doped fibers, so the spectral model is local in nature. The different spectral models are as follows (progressing from fastest/least accurate to slowest/most accurate):

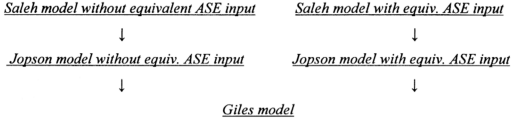

If the user selects the Giles model, it first solves the fiber using the Saleh model with equivalent ASE, then uses that as a first guess in the Jopson model, which is then passed as a first guess to the Giles model. Note that the Jopson model is the same, with or without ASE. If the user specifies the Jopson model without equivalent ASE input, it first solves the system using the Saleh model without equivalent ASE input, and then passes that solution to Jopson's model.

For each doped fiber, the user also specifies the mode approximation and number of transverse integrations, again trading off speed and accuracy. These factors are local to each doped fiber, so different doped fibers can have different degrees of accuracy. For each algorithm, the sources are calculated first, then all of the passive components, the doped fibers, and the receivers. This process is repeated, until the maximum number of iterations is reached.

2.9.2 Simulation Setup

Fig. 2.7 shows the configuration of an EDFA without feedback used in the simulation. The optical signal was provided by a tunable laser source (TLS) and was coupled to the EDFA system through a wavelength division multiplexer (WDM). The amplified signal was monitored by an optical spectrum analyzer (OSA). An erbium-doped fiber (EDF) was pumped by a laser diode (LD) at 980.1 nm. Two fiber couplers (C1 and C2) with a coupling ratio of 95% were spliced to the system in order to

compare with the experimental configuration as shown in Fig. 3.1. Giles parameters used in the simulation are listed in Table 2.1.

Table 2.1 Giles parameters

Core radius	1.68 μm
Er radius	1.68 μm
Ion density	5.76^{+24} m^{-3}
Loss at 1300 nm	20 dB/km
Metastable lifetime	10 ms
Numerical Aperture	0.24
Length	15 m
Calculation algorithm	Giles
Geometry model	LP01
Confinement factor	Power independent
Rayleigh backscattering constant	150dB/km
Back scatter capture	0.1%
Concentration quenching	None/Inhomogeneous/Homogeneous/Combined
Ions per cluster	2
Relative number of clusters	12%

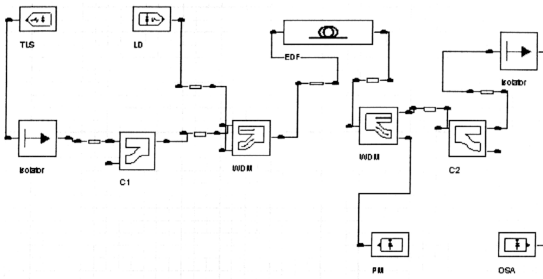

Fig. 2.7 *Setup used for simulation using OptiAmplifier. (TLS: tunable laser source; LD: laser diode; EDF: erbium-doped fiber; C: coupler; WDM: wavelength division multiplexer; PM: power meter; OSA: optical spectrum analyzer)*

2.9.3 Comparison of Simulation Results with Experimental Results

Based on the Giles model, simulation results are compared with experimental results in this section. Data for different concentration quenching effects, namely *inhomogeneous*, *homogeneous*, *combined* and *none*, are presented in order to choose the most accurate quenching effect from the simulation. Figs. 2.8(a) and (b) show the gain and noise figure of the EDFA, respectively, as a function of pump power with a constant input signal of –32.2 dBm. Filled circles represent the experimental data while the lines represent the simulation results. The figure shows that degree of deviation of the simulation results from the experimental data is dependent on the quenching effect chosen. The assumption that the active medium is homogeneously broadened is proved to be inappropriate since the discrepancy is large especially at the

low pump region. In the actual case, defects, dislocations, or lattice impurities in host crystals and the amorphous structure of glass hosts lead to site-to-site variations of the surrounding field and cause a randomization of the Stark effect, changing the energy positions of the Stark sublevels. Furthermore, site-to-site variations and existence of multiple types of sites in the host cause the activators to exhibit different laser line characteristics. Therefore, there will be shifts in the energy levels of the ion and the fluorescence or absorption observed from this collection of ions will be smeared by the *inhomogeneous broadening*. By considering this effect, the simulation results show a better agreement with the experimental data as compared to those of homogeneous effect and combination of homogeneous and inhomogeneous effect (*Combined*). However, Er^{3+} ions density of +440 ppm ($5.76\ ^{+24}\ m^{-3}$) is relatively low to cause the *homogeneous* and *inhomogeneous* effects. Without taking into account these effects (*None*), the simulation results are in good agreement with the measurement results.

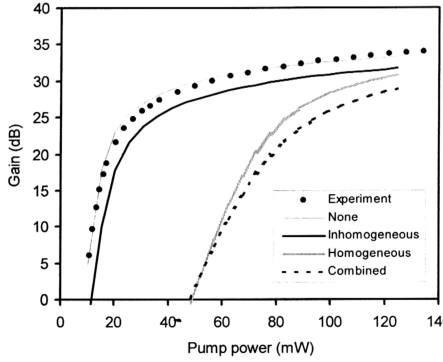

(a)

(continue...)

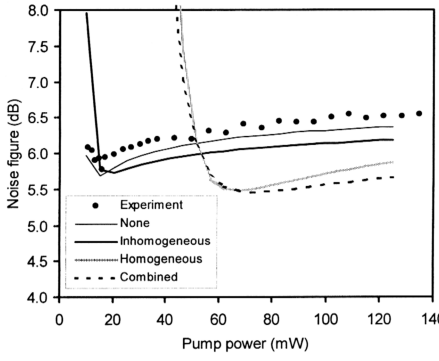

(b)

Fig. 2.8 *(a) Signal gain and (b) noise figure as a function of pump power with the input signal level of –31.2 dBm. Different concentration quenching effects, namely homogeneous, inhomogeneous, combined and none, are considered in the simulation for comparing with the experimental data.*

Figs. 2.9(a) and (b) show gain and noise figure, respectively, as a function of input signal power at the maximum pump power of 134.5 mW. Without considering the concentration quenching effects, the simulation results and the experimental results for the signal gain are in good agreement, especially in the saturation regime. However, there is a small discrepancy in the small signal regime. By considering the concentration quenching effects, discrepancy between the simulation and the measurement is relatively large. In the case of noise figure, a good agreement is

achieved only in the small signal regime without considering the concentration quenching effect. However, in the saturation regime, the discrepancy is large.

Overall, the modeling results are closely emulating the experimental data if quenching effect is not taken into account. Therefore, in Chapter IV, V and VI, the simulation results are all based on the assumption that no concentration quenching effects come into play.

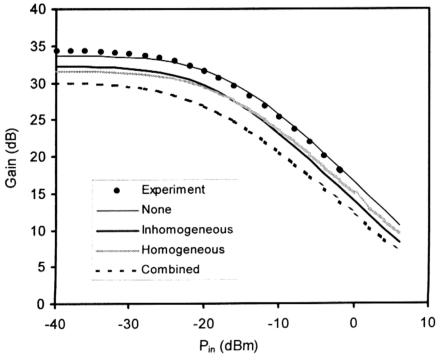

(a)

(continue...)

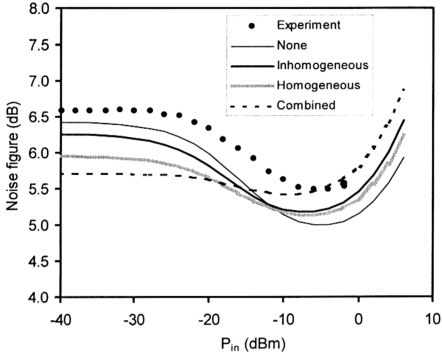

(b)

Fig. 2.9 *Comparison between simulation and measurement at the pump power of 134.5 mW. (a). Signal gain and (b). noise figure as a function of input signal power.*

REFERENCES

[1] Shoichi Sudo, "Optical fiber Amplifier: Materials, Devices, and Applications," Artech House, Inc, 1997.

[2] G. H. Dieke and H. M. Crosswhite, "The spectra of the doubly and triply ionized rare earths," Appl. Opt., 2, pp. 675, 1963.

[3] S. Hufner, "Optical Spectra of Transparent Rare Earth Components," Academic Press, 1978.

[4] M. J. Weber, "Fluorescence and glass lasers," J. Non-Cryst. Solids, 47, pp. 117, 1982.

[5] E. Desurvire, "Erbium-doped Fibre Amplifiers: Principles and Applications," John Wiley, Sonc, Inc, 1994.

[6] M. J. Weber, "Radiative and Multiphonon Relaxation of Rare-Earth Ions in Y_2O_3," Phys. Rev., 171, pp. 283, 1968.

[7] L. A. Riseberg and H. W. Moos, "Multiphonon orbit-lattice relaxation of excited states of rare earth ions in crystal," Phys. Rev., 174, pp. 429, 1968.

[8] R. Reisfeld and C. K. Jorgensen, "Lasers and Excited States of Rare Earths," Springer-Verlag, pp. 82, 1977.

[9] L. A. Riseberg and H. W. Moos, "Multiphonon orbit-lattice relaxation of excited states of rare earth ions in crystal," Phys. Rev., 174, pp. 429, 1968.

[10] M. Horiguchi, K. Yoshino, M. Shimizu, M. Yamada and H. Hanafusa, "Erbium-Doped Optical Fiber Amplifiers Pump in the 660- and 820-nm Bands," J. Lightwave Technol., 12, pp. 810, 1994.

[11] M. Yamada, M. Shimizu, M. Okayasu, T. Takeshita, M. Horiguchi, Y. Tachikawa and E. Sugita, "Noise Charateristics of Er^{3+}-Doped Fiber

Amplifiers Pumped by 0.98 and 1.48 μm Laser Diodes," IEEE Photon. Technol. Lett., 2, pp. 205, 1990.

[12] E. Desurvire and J. R. Simpson, "Amplification of Spontaneous Emission in Erbium-Doped Single-Mode Fibers," J. Lightwavw. Technol., 7, pp. 835, 1989.

[13] W. J. Barnes, R. I. Laming, E. J. Tarbox, and P. R. Morkel, "Amplification and Emission Cross Section of Er^{3+} Doped Silica Fibers," IEEE J. Quantum Electron., 27, pp. 1004, 1991.

[14] T. C. Teyo, M. K. Leong and H. Ahmad, "Lasing wavelength dependence of gain clamped EDFA performance with different optical feedback schemes," accepted to be published in Opt. & Laser Technol.

[15] T. C. Teyo, M. K. Leong and H. Ahmad, "Noise Characteristics of Erbium-doped Fiber Amplifier With Different Optical Feedback Schemes," Opt., Comm., 207, pp. 327, 2002.

[16] Tuan Chin TEYO, Mun Kiat LEONG and Harith AHMAD, "Noise Characteristics of Erbium-Doped Fiber Amplifier with Optical Counter-Feedback," Jpn. J. Appl. Phys., 41, 5A, pp. 2949, 2002.

[17] A. E. Siegman, Lasers, University Science Books, CA, 1986..

[18] D. Derickson, "Fiber Optic Test and Measurement," Prentice Hall, 1998.

[19] M. Cai, X. Liu, J. Cui, P. Tang, and J. Peng, "Study on noise characteristic of gain-clamped erbium-doped fiber-ring lasing amplifier," IEEE Photon. Technol. Lett., 9, pp. 1093, 1997.

[20] OptiAmplifier User's Guide, Version 3, OptiWave Corp., 2002.